

Nanoclay Exfoliation in Rubber Compounds Characterized by Online Measurements of Electrical Conductance

Zulfiqar Ali,¹ Hai Hong Le,¹ Sybill Ilisch,¹ Karsten Busse,² Hans-Joachim Radusch¹

¹Center of Engineering Sciences, Polymer Technology, Martin Luther University Halle-Wittenberg, D-06099 Halle, Germany

²Institute of Chemistry, Physical Chemistry of Polymers, Martin Luther University Halle-Wittenberg, D-06099 Halle, Germany

Received 22 September 2008; accepted 14 December 2008

DOI 10.1002/app.29914

Published online 23 March 2009 in Wiley InterScience (www.interscience.wiley.com).

ABSTRACT: A new method based on the online measured electrical conductance is presented for the characterization of the kinetics of dispersion of organoclay in a polar rubber matrix during melt mixing. The charge carriers available in the clay galleries become released as a result of the dispersion processes; thus, the conductance of the nanocomposites is altering during mixing. A coupled conductance/temperature sensor installed inside the mixing chamber enables the online measurement of the electrical conductance during mixing. The online measured conductance shows a characteristic chart correlating to the nanoclay dispersion process. To clarify the structural background of the conductance curve the kinetics of macro- and microdispersion of nanoclay have been investigated with the use of optical microscopy, small-angle X-ray diffraction (SAXS),

and atomic force microscopy (AFM), as well as bound rubber measurements. A close correlation was found between the online conductance chart and the development of the clay dispersion. In the first mixing step, breakdown of agglomerates, diffusion of polymer chains into the galleries of the clay, wetting, and intercalation processes take place simultaneously. As a result, a significant increase of conductance is observed during this period. Subsequently, the intercalated structures undergo the exfoliation process, which causes a further but moderate increase of the electrical conductance. © 2009 Wiley Periodicals, Inc. *J Appl Polym Sci* 113: 667–677, 2009

Key words: nanocomposites; rubber; clay; electrical conductance; online measurement

INTRODUCTION

Spherical nanofillers like carbon black (CB) or silica have been used in rubber compounds for more than 50 years. During the last 10 years, nanoclay has gained increasing interest as filler for rubber because of its specific properties. Nanoclay consists of anionic-charged layers of aluminum/magnesium silicates and small cations such as sodium or potassium located in silicate interlayer galleries.^{1,2} These cations can be exchanged with organic cationic molecules. The modification of the pristine clay by such surfactants, e.g., organic ammonium ions expands the layer spacing and makes the clay more compatible to the polymer matrix.³

Intercalated structures are formed when segments of the macromolecules infiltrate the expanded layers. Exfoliated structures are formed when the clay layers are well separated and individually dispersed in the

polymer matrix. The intercalation/exfoliation of clay platelets in the polymer matrix results in improved mechanical properties,^{4,5} e.g., increased storage and loss moduli⁶ or improved stiffness,⁷ reduced gas permeability,^{8,9} increased thermal stability,¹⁰ and improved flame retardance.¹¹ The main reasons for the improved properties of nanoclay-filled composites with respect to the bulk polymer are the large aspect ratio of the layers having a few nanometer thickness and dimensions in the micrometer range in the other two directions, the very large inner surface, as well as the strong interactions with polymer. Thus, the effectiveness of nanoclay for polymers strongly depends on its dispersion in the polymer matrix and especially on its degree of intercalation and exfoliation.

Different attempts in terms of variation of rubber matrix or chemistry of nanoclay have been made to disperse clay platelets in rubber compounds to get improved properties.¹² Jacob et al.¹³ prepared natural rubber (NR) clay–nanocomposites by using different concentrations of clay and showed the formation of an intercalated structure. Wu et al.¹⁴ reported that carboxylated acrylonitrile-butadiene rubber (XNBR) – clay nanocomposites exhibit a total exfoliated state. However, Sahdu,¹⁵ using transmission electron microscopy (TEM) and atomic force microscopy

Correspondence to: H.-J. Radusch (hans-joachim.radusch@iw.uni-halle.de).

Contract grant sponsors: German Research Foundation (DFG), Higher Education Commission Pakistan (HEC).

(AFM) could show that hydrogenated acrylonitrile-butadiene rubber (HNBR) forms with clay intercalated and exfoliated structures both with the unmodified and the modified clay. Kim et al.¹⁶ investigated the effect of the chain length (number of carbon atoms) of the surfactant on the clay dispersion in NBR and found that clay modified with C8-surfactants shows an intercalated structure whereas C12 and C18 surfactants modified clay exfoliates fully in NBR. Recent studies have demonstrated that beside the proper choice of materials, the conditions of processing play a key role in achieving exfoliation.^{17–20} Despite the current progress in polymer nanocomposite technology, there are many fundamental unanswered questions related to the kinetics of intercalation and exfoliation processes. It is fact that the development of an online (in situ) method would provide desirable and efficient feedback which can be used to understand the relationship between the various factors affecting the clay dispersion and to control the product quality.

Some authors^{21–24} have reported the appearance of a conductance signal while manufacturing polymer-nanoclay nanocomposites. Kortaberria et al.²² and Hussain et al.²³ as well as Jang et al.²¹ used dielectrical measurements for the characterization of the curing kinetics of epoxy matrices modified with organoclay. They showed that an addition of organoclay alters the conductivity properties of the epoxy matrix. Greater conductivity values have been obtained for greater clay contents. They suggested that the conductivity exists because of the high ion transfer through the inter- and intra-region of silicate galleries. By using online dielectrical measurements, Bur et al.^{25,26} detected electrical signals of polyamide (PA)–clay composites during the extrusion process. They supposed that the appearance of conduction may be related to the change of the microstructure of the composites. Aranda et al.²⁴ characterized the ionic conduction mechanism of intra-crystalline polymer–salt complexes obtained by insertion of poly(ethylene oxide) (PEO) and crown ether compounds in an unmodified clay containing Na⁺ exchangeable cations in their interlayer space. PEO compounds (crown ethers and PEO) are able to associate interlayer Na⁺ cations by modifying dramatically the ionic conductivity of the natural silicate. The conductivity of these compounds with intercalated clay structures depends on the interaction strengths between the interlayer Na⁺ cation and the oxyethylene compound. Macrocyclic polyethers that form very stable complexes restrain the Na⁺ ion mobility and, consequently, the electrical conductivity observed is low. PEO involves weaker cation interactions, which can be invoked to explain the significant enhancement of the conductivity found. It is noteworthy that in these materials the contribution of the anions to the ionic conductivity

can be considered 0 because the negatively charged silicate layers constitute the anionic entities and, consequently, the transport cationic number for these systems must be assumed to be unity, in view of the immobility of the anions.²⁴ This situation is quite different to conventional PEO salt complexes, where an organic macromolecule acts as a solvent of the salt and dissociates partially, making it possible for the system to operate as a mixed cationic/anionic ion-conductor. Thus, in the intercalated materials presented by²⁴ exclusively cationic conductivity takes place.

On the basis of the idea that the electrical conductivity of the compound represents a function of the dispersion and distribution of a conductive filler, we have developed a method that uses the electrical conductance measured online directly in the mixing equipment in dependence on the mixing time. This method has been successfully used for the qualitative and quantitative characterization and description of the kinetics of CB and carbon nanotube dispersion and distribution in rubbers and rubber blends.^{27–33} As mentioned previously, the addition of organoclay changes the conductivity properties of the host polymer as a result of the additional ionic charge carriers available from the clay. Regarding this, we presumed that along the mixing time nanoclay undergoes different dispersion stages that releases charge carriers trapped inside the clay galleries. Thus, the received electrical signal can be used for the investigation of the change of the clay dispersion in the host polymer during the mixing process as shown in our preliminary work.³⁴ In the present work, the correlation between the electrical conductance online-measured directly in a chamber of an internal mixer during the preparation of rubber-clay nanocomposites and the macro- and micro-dispersion as well as the intercalation and exfoliation of clay will be discussed.

EXPERIMENTAL

Materials and preparation of rubber-clay nanocomposites

XHNBR Therban XT VP KA 8889 (Lanxess, Leverkusen, Germany) with an acrylonitrile content of 33% was used as a host polymer. Organoclay Nanofil 9 (Süd-Chemie, Moosburg, Germany) modified by steryl benzyl dimethyl ammonium chloride with layer spacing of 2.0 nm, an average particle size of about 35 μm , and a weight loss on ignition of 35% was used as the modified nanofiller and Na-nanoclay Cloisite Na⁺ (Southern Clay Products) with a weight loss on ignition of 7% as the unmodified filler. Peroxide Luperox 101 (Atofina Chemicals) was used as a cross-linking agent.

XHNBR was mixed with peroxide in an internal mixer PolyLab System Rheocord (Thermo Electron/Haake, Karlsruhe, Germany) at an initial chamber temperature of 50°C and a rotor speed of 70 rpm. Clay was added after 7 min. A clay concentration of 5 phr was kept constant for all nanocomposites. For the characterization of the dispersion kinetics of nanoclay samples were taken out after different mixing times of 1, 3, 4, 10, 25, and 30 min. The mixing time denotes the time after addition of nanoclay. A reference series was also prepared by a rotor speed of 25 rpm, and an initial chamber temperature of 70°C was chosen in order to keep the mass temperature similar for both series. For a second series, the mixtures were prepared for different time intervals of 10 s, 1, 2, 7, 10, 20, and 45 min. The mixtures were compression-molded and vulcanized for 1-mm-thick plates.

Online electrical conductance measurements

A conductivity sensor has been installed in the chamber of the internal mixer to measure the conductance signal of the mix volume between the sensor and the chamber wall as used in.³² The construction and position of the conductivity sensor was modified to detect the conductance signal of the investigated system with good reproducibility. The online measured electrical conductance is called online conductance from this point forward.

Morphological Investigations

Optical microscopy

Optical microscopy has been used to characterize the macrodispersion of nanoclay in rubber. This method was described by Leigh-Dugmore³⁵ for CB and modified by us for nanoclay. The dispersion degree A/A_0 is the ratio of the area of the nondispersed tactoids of clay with an average diameter greater than 3 μm and the total area of the image.

Atomic force microscopy

Morphological investigations were conducted by an atomic force microscope Q-Scope 250 (Quesant, Santa Cruz, CA), operated in intermittent mode with a scan head of 40 μm . Samples were produced by cutting in a cryo-chamber CN 30 of a rotary microtom HM 360 (Microm, Walldorf, Germany) with a diamond knife at -120°C .

Transmission electron microscopy

Microstructure was examined using a TEM microscope, JEM 2010 (JEOL, Tokyo, Japan). Ultrathin sections of each sample (ca. 100 nm) were prepared at

-100°C from a bulk specimen using an ultramicrotome Ultracut E (Leica, Wetzlar, Germany) with cryo-system FC6 (Leica).

Measurement of rubber layer bound on the nanoclay surface

On the basis of our developed method,³⁶ the characterization of the wetting behavior of nanoclay by rubber chains was realized. When nanoclay is mixed with a rubber, a part of the rubber chains will be bonded to the existing reactive groups which are available on the surface of nanoclay. Extracting the filled, unvulcanized raw rubber compound with acetone, the bound part of the rubber forming a layer around the filler particles remains in the rubber-filler gel. The determination of the amount of rubber L bound to the surface of the nanoclay was carried out according to eq. (1).³⁶

$$L = \frac{m_2 - m_1 \cdot c_R}{m_2} \quad (1)$$

The mass m_1 corresponds to the rubber compound before extracting; it is the sum of the mass of the undissolvable rubber, the mass of the soluble rubber, and of nanoclay. m_2 is the mass of the rubber-filler gel, which is the sum of the undissolvable rubber and the mass of nanoclay. c_R is the mass concentration of nanoclay in the mixture. This value is dimensionless and lies between 0 and 1. For the experimental work, 0.25 g of the uncured mixture were stored at room temperature in 100 mL of acetone. After 3 days, the rubber-filler gel was taken out and dried up to a constant mass.

Thermogravimetric analysis

The thermogravimetric analysis of the nanoclay and the rubber-filler gel was conducted with a thermobalance TGA /SDTA 851 (Mettler-Toledo). The samples were heated up to 800°C with a heating rate of 20 K/min in air atmosphere. The loss of sample weight was recorded.

X-ray diffraction

Small-angle X-ray scattering (SAXS) measurements were performed at room temperature using a rotating anode X-ray source RU-3HR (Rigaku) equipped with a nickel-filtered Cu $K\alpha$ tube ($\lambda = 0.154 \text{ nm}$) for detection of the state of exfoliation. The generator voltage was 40 kV, and generator current was 60 mA. The scattering vector q is defined by $q = 4\pi/\lambda \sin \theta$. The first-order Bragg peak in the Lorentz corrected intensity curves was fitted by the use of a Gaussian function with linear background subtraction, giving the interlayer distance and the relative

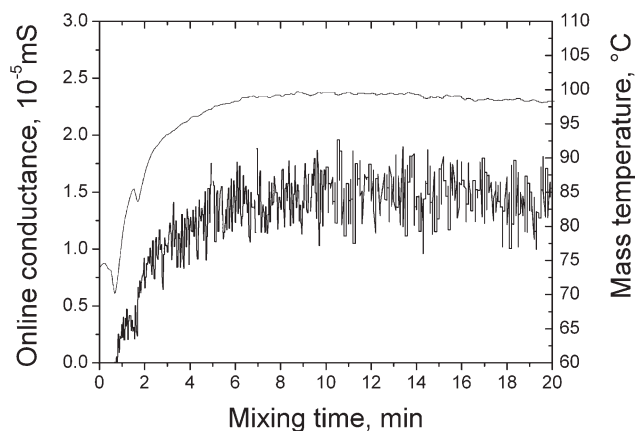


Figure 1 Online conductance of pure XHNBR.

peak strength. All samples had a uniform thickness of 1.0 mm, i.e., the obtained peak area corresponds to the amount of ordered structures.

Tensile properties

The tensile modulus was determined by stress–strain measurements according to DIN EN ISO 37 using a tensile tester Z005 (Zwick/Roell) at room temperature. The test specimens have a thickness of 1 mm and an initial length of 50 mm. All data presented are the average of five measured specimens for each sample.

RESULTS AND DISCUSSION

The online conductance chart of rubber-clay nanocomposites

The online measured electrical conductance curve of pure XHNBR versus the mixing time is shown in Figure 1. When the rubber was filled into the chamber, the online conductance increased to a certain value and then remained constant. The increasing conductance is in line with the increasing mass temperature which, on the one hand, causes a better contact between rubber and the sensor and intensifies, on the other hand, the transport process of the low amount of charge carriers contained in the rubber. The material is masticated and the online conductance reaches its optimum value after 7 min; meanwhile, the temperature also becomes constant. XHNBR contains highly polar nitrile groups on the main chain. These groups may act as electron-rich centers; thus, they will influence the transfer of charge carriers as the result of polarization and alignment opposing to the external applied electric field.

In the simplest quantitative form the electrical conductance can be expressed by eq. (2).

$$\sigma = n \cdot e \cdot \mu \quad (2)$$

where n is the number of charge carriers per unit volume, e is the electronic charge, and μ is the mobility of the carrier.

Figure 2 depicts the development of the online conductance when adding nanoclay into the XHNBR rubber matrix by the rotor speed of 70 rpm [Fig. 2(a)] and of 25 rpm [Fig. 2(b)]. The mixing time indicated in these figures is the time after nanoclay addition. The difference between the unmodified Na^+ nanoclay and the organoclay is presented. Although the unmodified Na^+ -nanoclay does not show any electrical signal [Fig. 2(a)], the conductance of modified clay increases significantly and passes through two distinct points, which are assigned as the characteristic point 1 (CP 1) at 3 min and characteristic point 2 (CP 2) at 12 min before it reaches a plateau. In the stage up to CP 1, a sharp increase of the conductance is observed. The development of the conductance decreases in the stage between CP 1 and CP 2. After CP 2 no change of the conductance is observed. When the rotor speed reduces to 25 rpm

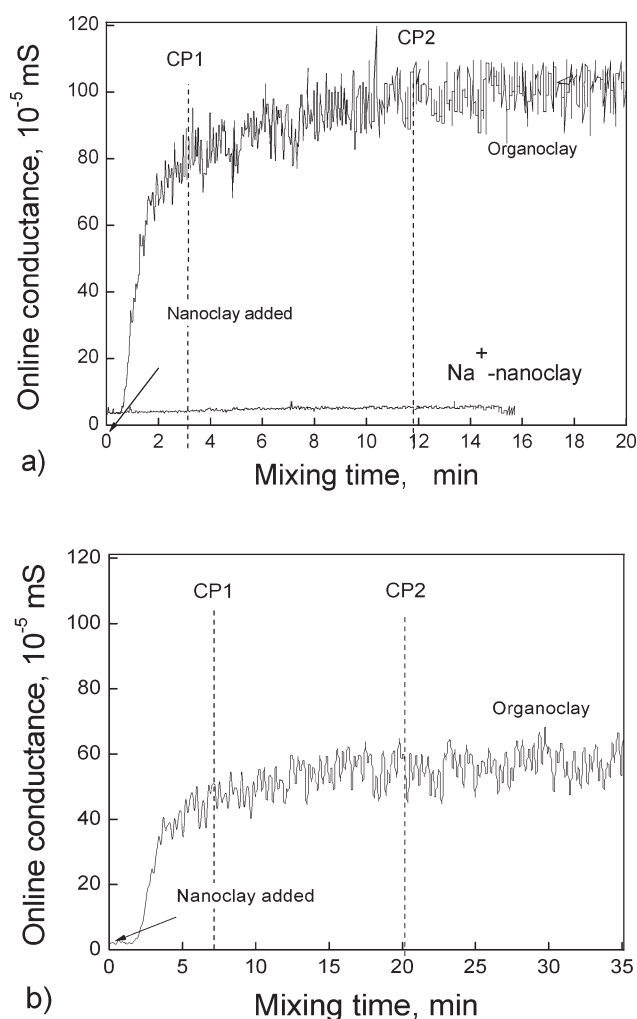


Figure 2 Online conductance of XHNBR-clay composites mixed by the rotor speed of 70 rpm (a) and 25 rpm (b).

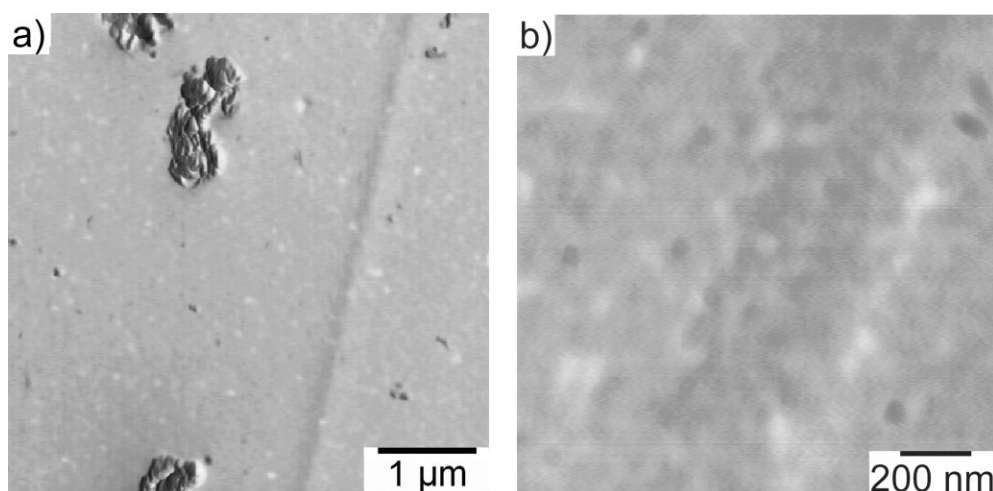


Figure 3 AFM images of XHNBR-Na⁺-nanoclay composite at different magnification.

[Fig. 2(b)], the conductance curve is reduced to a lower level and prolonged, and a CP 1 of 7 min and CP 2 of ~ 20 min were observed. Considering the relevant literature the rapid increase of the conductive signal just after adding nanoclay could be attributed to the ionic conduction. The modified clay is organophilic with a lower surface energy and, therefore, it is more compatible with organic polymers. As a result, the polymer chains intercalate within the galleries. Because the nitrile group of XHNBR is a strong electron donor, a hydrogen-bond formation between the ammonium ion of the intercalated amine and the nitrile group exists.³⁷ That seems to disassociate or weaken the attractive force between the cationic head group of the alkylammonium molecule and the negatively charged clay surface. The steady motion of rubber chains during the mixing facilitates the displacement of quaternary ammonium ions from one nitrile group to the other. Thus, even a large cation like alkylammonium could move easily in the rubber matrix, causing an increase of conductance by two orders of magnitude compared with that of the plain XHNBR. The more the contact area between nanoclay and rubber increases along the mixing time because of the running intercalation and exfoliation processes, the more charge carriers release the clay galleries and impart the matrix a greater electrical conductance.

The online conductance of a rubber nanocomposites σ_{comp} (e.g., clay modified XHNBR) measured in the mixing chamber is the sum of both the electronic conductance of the rubber σ_{rubber} and the ionic one of the clay σ_{clay} as given in eq. (3).

$$\sigma_{\text{comp}} = \sigma_{\text{rubber}} + \sigma_{\text{clay}} \quad (3)$$

The absence of conductance in the case of the unmodified clay (Na⁺-nanoclay) as shown in Figure 2(a) can be explained by the fact that layered sili-

cates are naturally hydrophilic, with Na⁺ cations bonded between the sheets of oxygen and silicon. Such unmodified layered silicates have an interlayer spacing of ~ 1.2 nm. Therefore, as expected, the hydrophilic nature of Na⁺-nanoclay is hardly to intercalate by the bulky chains of XHNBR. Thus, by compounding with XHNBR, the unmodified Na⁺-nanoclay particles are simply incorporated into the rubber matrix in an agglomerated state as shown in Figure 3(a), where some tactoids of Na⁺-nanoclay are visible. Also the AFM image with greater magnification does not show any separated nanolayers [Fig. 3(b)]. Compared with the interlayer spacing of ~ 1.2 nm before compounding, the interlayer spacing of ~ 1.3 nm after compounding observed in unmodified NBR and NR/EVA composites³⁸ means that no intercalation process took place. In this case,

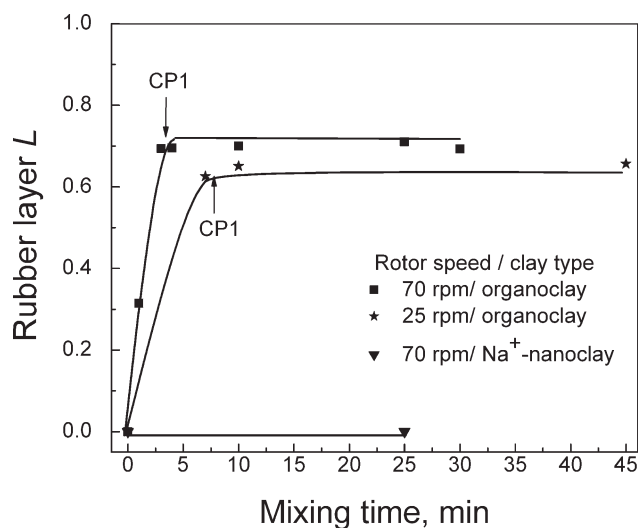


Figure 4 Rubber layer L bound on the clay surface of the mixture versus mixing time for different rotor speeds and clay types.

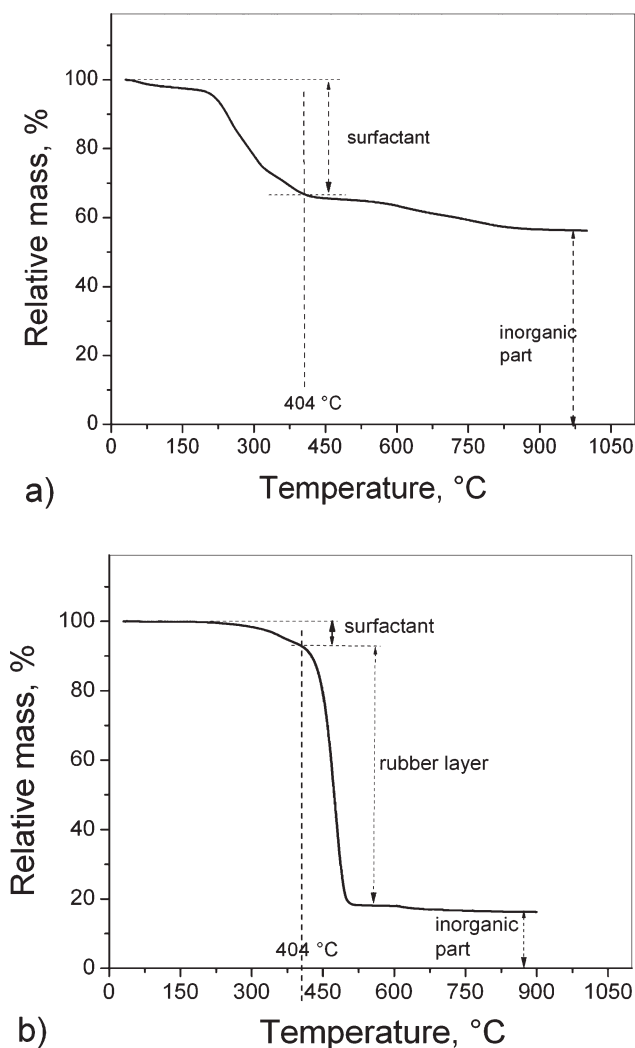


Figure 5 Thermogravimetric analysis of organoclay (a) and the rubber-filler gel (b) extracted from the sample taken out at 10 min mixing time.

Na^+ cations are trapped inside the clay galleries explaining why no electrical signal was observed in the XHNBR mixtures. Otherwise, the Na^+ -nanoclay/PEO compound mentioned above²⁴ was prepared by a solution process that allows PEO to intercalate Na^+ -nanoclay. Such intercalated state imparts the nanocomposite ionic conduction due to the mobility of Na^+ ions.

Characterization of the structural background of the online conductance chart

The determination of the rubber layer L bonded on the nanoclay surface for different nanocomposites was realized using eq. (1). The results for different XHNBR-clay compounds are shown in Figure 4.

For organoclay composites, the amount of rubber layer L increases strongly in the stage up to CP1 at 3 and 7 min of the mixture mixed at 70 and 25 rpm, respectively. The fast increasing rubber layer L indi-

cates that the rubber chains diffuse very fast into the clay gallery, intercalate them, and wet their surface. After CP1, the rubber layer L reaches a plateau for both rotor speeds, indicating that all the surface of nanoclay is already wetted and even the exfoliation process yet goes on. It can be assumed that the intercalation is widely progressed or nearly completed at CP1. The value of L of the mixture mixed at 25 rpm is lower than that mixed at 70 rpm. This is related to the effectivity of the intercalation/exfoliation process when mixing with higher rate of energy input.³⁹ In the case of Na^+ -nanoclay composites, if XHNBR molecules are not able to intercalate and wet Na^+ -nanoclay as discussed above, the rubber layer L remains zero even after a longer mixing time (Fig. 4).

The results of the thermogravimetric analysis of the organoclay and the rubber-filler gel are presented in Figure 5(a and b), respectively. The relative mass loss W_S of 34% in the temperature range up to 404 °C is attributed to the degradation of the surfactant

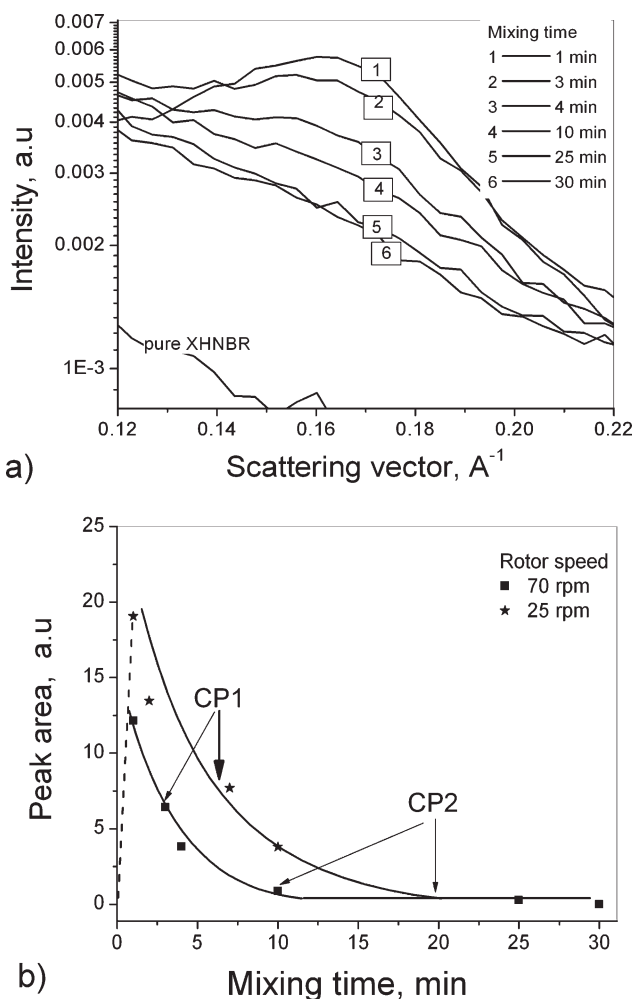


Figure 6 SAXS analysis (a) of pure XHNBR and XHNBR-organoclay mixtures after different mixing times mixed at 70 rpm and the area under the peak for both rotor speeds (b).

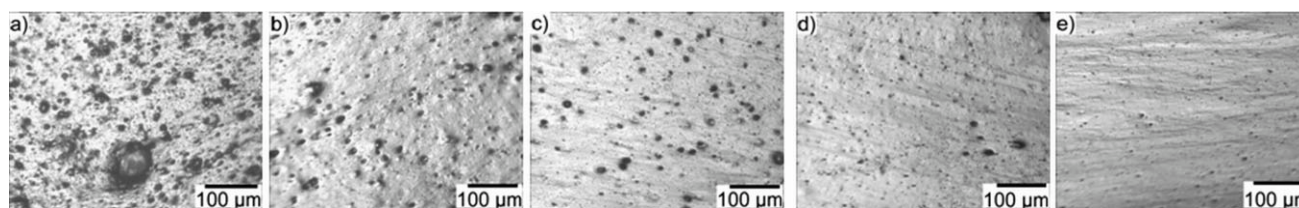


Figure 7 Development of morphology investigated by optical microscopy for XHNBR-organoclay composites mixed at 70 rpm, 1 min (a), 3 min (b), 4 min (c), 10 min (d) and 25 min (e).

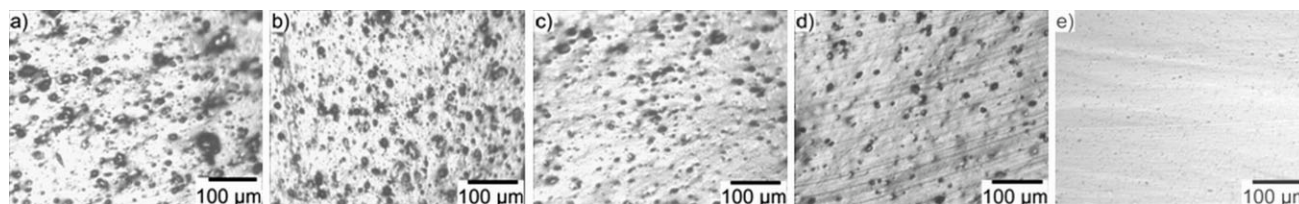


Figure 8 Development of morphology investigated by the optical microscopy for XHNBR-organoclay composites mixed at 25 rpm, 1 min (a), 3 min (b), 7 min (c), 10 min (d) and 45 min (e).

[Fig. 5(a)]. The inorganic part of the organoclay W_I of 66% was identified as the material remained beyond 600°C presented. Analyzing the relative mass curve of rubber-filler gel reveals two distinct degradation processes [Fig. 5(b)]. In the temperature range up to 404°C the surfactant degrades first. Its corresponding mass loss W_S is 7%. In the subsequent temperature range between 404 and 507°C XHNBR degrades. The mass loss of ~ 74% in this range corresponds to the rubber layer L presented in Figure 4. W_I of the inorganic part of the organoclay in the rubber-filler gel amounts 19%. The ratio can be used as a measure to determine the loss of the surfactant if it releases the organoclay galleries. The ratio W_S/W_I of 0.5151 and 0.3684 was calculated for organoclay and rubber-filler gel, respectively. That means that the surfactant that remains inside the clay galleries after mixing amounts only three-fourth of that of the initial organoclay. One-fourth of the surfactant already was released and moved into the rubber matrix causing an ionic conductance. During the extraction experiment of the rubber-filler gel the released surfactant was extracted together with the unbound rubber.

The SAXS analysis in Figure 6(a) shows curves of the nanocomposites with large broad peaks representing the interlayer spacing of the nanoclay in the nanocomposites; they are changed in intensity with increasing mixing time. The position of the peaks, however, remains unchanged. The data of the clay provider as well as own investigations show that the organoclay has a basal spacing of 2.0 nm before compounding. The characteristic peak at the scattering vector $q = 0.159 \text{ \AA}^{-1}$ corresponds to a basal spacing of about 4.2 nm of the organoclay in the nanocomposites. The calculated area under the peak for both rotor speeds is presented in Figure 6(b). As the mixing time increases, the peak height and the

area under the peak for both rotor speeds decrease. The peak reaches the highest level after a mixing time of about 1 min due to the intercalation process. The following decrease of the peak height indicates that the regular structure in the nanocomposite is collapsed, i.e. delaminated, or the clay layers are homogeneously dispersed already. Consequently, it may be reasonable to mention that the nanoclays are exfoliated in the polymer matrix. As discussed above (Fig. 4), the intercalation process runs mainly up to CP 1. Thus, we can conclude that up to CP 1 both intercalation and exfoliation take place simultaneously and they affect the height of the peak in the opposite direction. Due to such an intensive intercalation and exfoliation process a larger amount of ionic species trapped inside the galleries could move now into the rubber matrix. This is the main reason

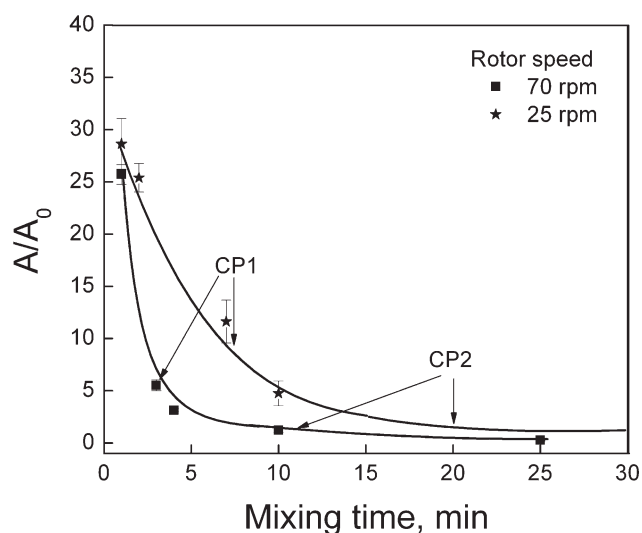


Figure 9 Macrodispersion of XHNBR-organoclay composites prepared at different rotor speeds.

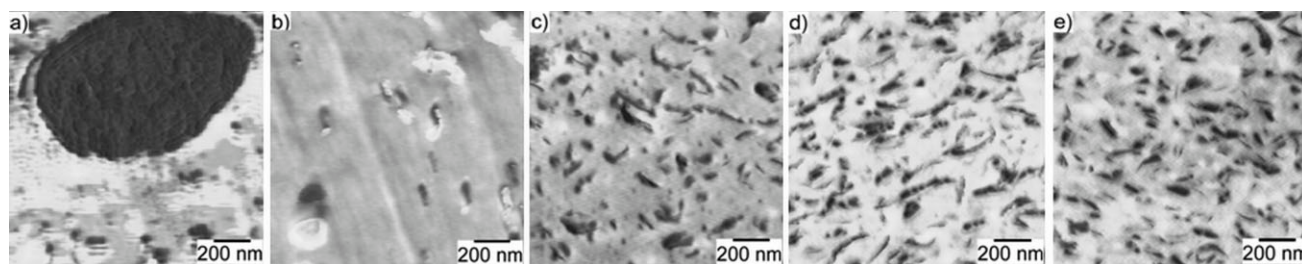


Figure 10 AFM images of XHNBR-organoclay composites mixed with a rotor speed of 70 rpm, 1 min (a), 3 min (b), 4 min (c), 10 min (d) and 25 min (e).

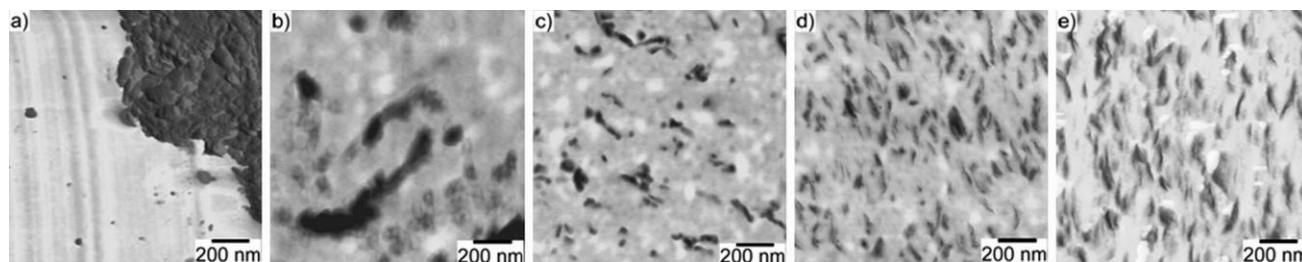


Figure 11 AFM images of XHNBR-organoclay composites mixed with a rotor speed of 25 rpm, 1 min (a), 3 min (b), 7 min (c), 10 min (d) and 45 min (e).

why the online conductance increases so fast in the first stage of the mixing process.

For both higher and lower mixing rate the area under the peak becomes approximately zero at the mixing time of 12 or 20 min, respectively. This corresponds to the position of the critical point CP 2 of the mixture mixed at 70 or 25 rpm, respectively. In the stage between CP 1 and CP 2 only the exfoliation process causes a moderated increase of the online conductance since the release of the ionic species is more convenient. The disappearance of the peak in the SAXS curve behind CP 2 means a constant morphology of totally exfoliated state which causes a constant conductance in this period (Fig. 2).

The correlation between the online conductance and nanoclay dispersion on macroscopic scale (macrodispersion) has been characterized by optical microscopy for both rotor speeds. The images of the compounds taken at different mixing times were made by use of the optical microscope and are presented in Figures 7 and 8 for the rotor speed of 70 and 25 rpm, respectively.

It is obvious that the number and size of the nanoclay agglomerates decrease along the mixing time because large clay agglomerates are ruptured into smaller aggregates (tactoids). When the size of tactoids is less than 3 μm , they become invisible in the optical micrographs; thus, they are considered as dispersed only macroscopically. The change of morphology of the compounds mixed at 25 rpm seems to be slowed down compared to that at 70 rpm. To quantify the morphology change of the mixture, the macrodispersion A/A_0 was calculated and presented

in Figure 9. With the mixing time the macrodispersion A/A_0 decreases sharply in the first period up to CP 1 and reaches a value of zero at the mixing time corresponding to the CP 2 for both rotor speeds. A value of zero means, that no more tactoids with a diameter larger than 3 μm are available.

The microdispersion of organoclay in rubber was characterized by AFM and is presented in Figure 10 for the rotor speed of 70 rpm and Figure 11 of 25 rpm, respectively. It can be seen that up to CP 1 the agglomerates are broken into small tactoids [Fig. 10(a,b)]. The break-up process of larger agglomerates fast establishes new clay surface that facilitates the

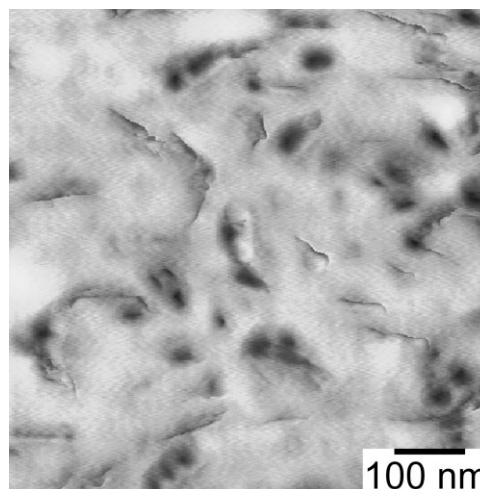


Figure 12 AFM images of XHNBR-organoclay composites mixed for 25 min with a rotor speed of 70 rpm.

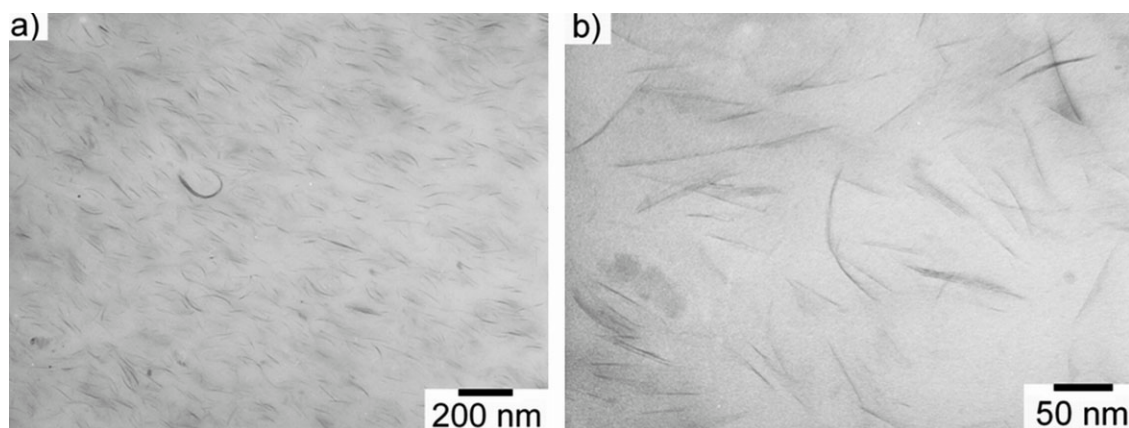


Figure 13 TEM images of XHNBR-organoclay mixtures mixed for 25 min with a rotor speed of 70 rpm at low (a) and high (b) magnification.

diffusion process of rubber chains into the clay gallery. As a result, in this period the intercalation and the wetting of clay surface by rubber molecules mainly take place, that has already been discussed above based on the SAXS analysis and bound rubber measurements (Figs. 4 and 6). In the period between CP 1 and CP 2 the number of separated nanolayer increases due to the exfoliation process [Fig. 10(c,d)]. Park and Jana⁴⁰ proposed in their study on epoxy nanocomposites that clay exfoliation starts at the surface layers of the tactoids and continues towards the center until all layers are exfoliated. Their proposed process is analog to the erosion process as described in the *onion model* used for the explanation of the dispersion process of carbon black in a polymer matrix.^{28,41} As visible in Figure 10(d,e), the morphology after CP 2 seems to remain unchanged that could explain the plateau of the online conductance in this period [Fig. 2(a)]. The constant conductance indicates that the clay dispersion has reached its final state. Further mixing only distributes the nanoclay layers more homogeneously in the polymer matrix. The microdispersion of the mixture prepared by the rotor speed of 25 rpm (Fig. 11) shows the similar tendency of the morphology change compared to the higher rotor speed (Fig. 10). However, at lower mixing rate dispersion needs longer mixing time due to the lower energy input.

It is worth to note that, according to SAXS analysis, no ordered structure exists in the period after CP 2. However, the separated nanolayers observed by AFM in Figure 10(d,e) as well as in Figure 12 have a thickness of ~ 30 nm. The reason for the large thickness measured in comparison to the theoretically expected one could be the existence of a rubber layer bound on the surface of the nanolayer. Because of its restricted mobility compared with unbound rubber, the rubber layer appears in AFM images as a shell surrounding the platelets. To confirm that the nanostructure of the samples was representative, one of the specimens

was characterized by means of TEM. The results are presented in Figure 13 on two magnifications. It is obvious that individual layers with a thickness of ~ 5 nm exist in the matrix. The bound rubber, however, is not visible in the TEM images because there is no contrast between the rubber matrix and the phase boundary layer formed by the bound rubber.

Mechanical modulus

The tensile modulus of polymer nanoclay composites is expected to depend on modulus of the polymer, modulus of the clay platelets, dispersion of the clay, clay loading, degree of crystallinity in the semi-crystalline polymer matrix, orientation of the clay tactoids or platelets, respectively, orientation of polymer crystallites, and interfacial stress transfer mechanisms. In the present work, the investigated systems show a continuous change of morphology from larger agglomerates through intercalated tactoids

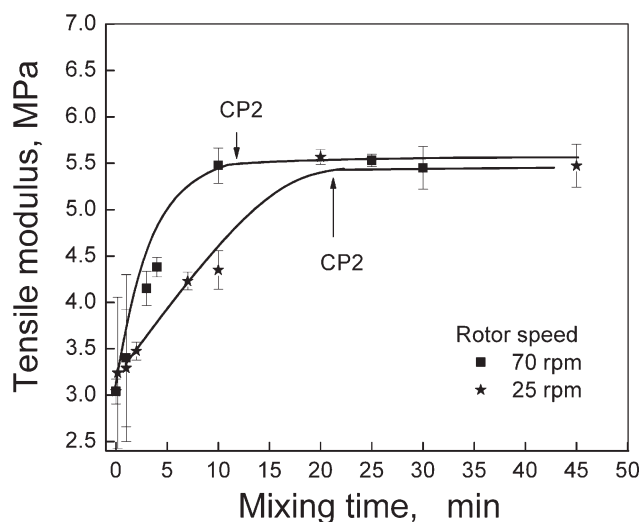


Figure 14 Tensile modulus versus mixing time and rotor speed for XHNBR-organoclay composites.





Mixing time	t=0	t = CP1	t = CP2	
Morphology				
Dispersion processes	Intercalation rupture erosion exfoliation	end of intercalation	exfoliation	end of exfoliation
OMEC		rapid increase	slow increase	plateau
Rubber layer L		rapid increase	plateau	
Macrodispersion		increase		plateau
Microdispersion	agglomerates	aggregates platelets		platelets
Tensile modulus		increase		plateau

Figure 15 Correlation between the dispersion processes of organoclay and the online conductance, rubber layer L , macro- and microdispersion, as well as the tensile modulus (schematic).

toward separated nanoplatelets along the mixing time. It is interesting to observe that the development of the tensile modulus changes in connection to the monitored online conductance curve and, of course, the morphology of the compound. In Figure 14, the tensile moduli of both series are presented in dependence on mixing time. For both rotor speeds the modulus increases with mixing time when the nanoclay undergoes different dispersion processes. The increase in the modulus is caused by the progressing intercalation and exfoliation that is consistent with the development of the online measured conductance values. The modulus reaches a plateau approximately at the CP 2 when the online conductance becomes constant and the morphology is fixed as well. An improvement of about 80% in the modulus was achieved when the nanoclay is more or less totally exfoliated. The lower rotor speed slows down the increase of modulus corresponding to the slower development of morphology finding its expression in the course of the conductance curve.

For a better understanding, the correlation between the dispersion processes of nanoclay and the online conductance, the rubber layer L , the macro- and microdispersion, as well as the tensile modulus is schematically presented in Figure 15.

CONCLUSIONS

Investigations on nanoclay (modified and unmodified)-filled XHNBR compounds have shown that it is possible to use the method of the online measured electrical conductance for the successful characterization of the kinetics of the dispersion processes during compounding of such polymer-nanofiller systems. Compound samples were taken out along the mixing time and analyzed by means of optical microscopy, AFM, TEM, and SAXS in terms of the dispersion and distribution of the nanoclay. Additionally, bound rubber measurements and mechanical tests performed provided a deeper insight into the mechanisms of the melt mixing process of nanoclay filled rubber. The strong correlation between the online measured electrical conductance and the filler dispersion delivered an effective tool for the investigation of the nanoclay dispersion (intercalation/exfoliation) in polymer melts.

We thank the companies Süd-Chemie/Germany for providing nanoclays and Lanxess/Germany for providing XHNBR.

References

- Ogawa, M.; Takizawa, Y. *Chem Mater* 1999, 11, 30.
- Wu, J.; Lerner, M. *Chem Mater* 1993, 5, 835.

3. Mittal, V. J *Therm Comp Mater* 2007, 20, 575.
4. Fornes, T. D.; Yoon, P. J.; Keskkula, H.; Paul, D. R. *Polymer* 2001, 42, 9929.
5. Reichert, P.; Nitz, H.; Klinke, S.; Brandsch, R.; Thomann, R.; Mülhaupt, R. *Macromol Mater Eng* 2000, 275, 8.
6. Gu, S. Y.; Ren, J.; Wang, Q. F. *J Appl Polym Sci* 2004, 91, 2427.
7. Gopakumar, T. G.; Lee, J. A.; Kontopoulou, M.; Parent, J. S. *Polymer* 2002, 43, 5483.
8. Lagaron, J. M.; Catala, R.; Gavara, R. *Mater Sci Technol* 2004, 20, 1.
9. Chang, J. H.; An, Y. U. *J Polym Sci Part B: Polym Phys* 2002, 40, 670.
10. Ma, J.; Qi, Z.; Hu, Y. *J Appl Polym Sci* 2001, 82, 3611.
11. Kandola, B. K.; Katsoulis, C.; Kandare, E.; Myler, P. *Fibre Reinforced Composites Conference, Port Elizabeth, South Africa, 2007*.
12. Bhowmick, A. K.; Ganguly, A.; Maiti, M. *Kautsch Gummi Kunstst* 2006, 59, 437.
13. Jacob, A.; Kurian, P.; Aprem, A. S. *Int J Polym Mater* 2007, 56, 593.
14. Wu, Y.; Jia, Q.; Yu, D.; Zhang, L. *J Appl Polym Sci* 2003, 89, 3855.
15. Sadhu, S.; Bhowmick, A. K. *J Mater Sci* 2005, 40, 1633.
16. Kim, J.; Oh, T.; Lee, D. *Polym Int* 2003, 52, 1058.
17. Cho, J. W.; Paul, D. R. *Polymer* 2001, 42, 1083.
18. Dennis, H. R.; Hunter, D. I.; Chang, D.; Kim, S.; White, J.; Cho, J. W.; Paul, D. R. *Polymer* 2001, 42, 9513.
19. Nah, C. W.; Ryu, H. J.; Han, S. H.; Rhee, J. M.; Lee, M. H. *Polym Int* 2001, 50, 1265.
20. Wang, K.; Liang, S.; Du, R. N.; Zhang, Q.; Fu, Q. *Polymer* 2004, 45, 7953.
21. Jang, W. Y.; Hwang, S. D.; Nam, J. D. Presented at the 33rd ISTC, Seattle, WA, November 5–8, 2001.
22. Kortaberria, G.; Solar, L.; Jimeno, A.; Arruti, P.; Gomez, C.; Mondragon, I. *J Appl Polym Sci* 2006, 102, 5927.
23. Hussain, F.; Chen, J. H.; Hojjati, M. *Mater Sci Eng A* 2007, 445, 467.
24. Aranda, P.; Galvan, J. C.; Casal, B.; Rue-hitzky, E. *Electrochim Acta* 1992, 37, 1573.
25. Bur, A. J.; Roth, S. C.; Lee, Y.; McBrearty, M. *Rev Sci Inst* 2004, 75, 1103.
26. Bur, A. J.; Lee, Y.; Roth, S. C.; Start, P. R. *Polymer* 2005, 46, 10908.
27. Le, H. H.; Ilisch, S.; Jakob, B.; Radosch, H.-J. *Rubber Chem Technol* 2004, 77, 147.
28. Le, H. H.; Prodanova, I.; Ilisch, S.; Radosch, H.-J. *Rubber Chem Technol* 2004, 77, 815.
29. Le, H. H.; Tiwari, M.; Ilisch, S.; Radosch, H.-J. *Kautsch Gummi Kunstst* 2005, 58, 575.
30. Le, H. H.; Tiwari, M.; Ilisch, S.; Radosch, H.-J. *Rubber Chem Technol* 2006, 79, 610.
31. Le, H. H.; Qamer, Z.; Ilisch, S.; Radosch, H.-J. *Rubber Chem Technol* 2006, 79, 621.
32. Le, H. H.; Wutzler, A.; Ilisch, S.; Radosch, H.-J. *Kautsch Gummi Kunstst* 2007, 60, 295.
33. Radosch, H.-J.; Le, H. H.; Ilisch, S.; Kasaliwal, G. In *Proceedings of Fibre Reinforced Composites Conference: Port Elizabeth, South Africa, 2007*; p 196.
34. Le, H. H.; Ali, Z.; Ilisch, S.; Radosch, H.-J. In *Proceedings of Technomer: Chemnitz, Germany, 2007*; p 29.
35. Leigh-Dugmore, C. H. *Rubber Chem Technol* 1956, 29, 1303.
36. Le, H. H.; Ilisch, S.; Kasaliwal, G. R.; Radosch, H.-J. In *Proceedings of Online Characterization of CNT Filled Rubber Compounds, PPS-24: Salerno, Italy, 2008*; p S18.
37. Sadhu, S.; Bhowmick, A. K. *J Polym Sci Part B: Polym Phys* 2004, 42, 1573.
38. Sharif, J.; Yunus, W. M. Z. W.; Dahlan, K. H.; Ahmad, M. H. *J Appl Polym Sci* 2006, 100, 353.
39. Vaia, R. A.; Jant, K. D.; Kramer, E. J.; Giannelis, E. P. *Chem Mater* 1996, 8, 2628.
40. Park, J.; Jana, S. *Macromolecules* 2003, 36, 8391.
41. Shiga, S.; Furuta, M. *Rubber Chem Technol* 1985, 58, 1.